ELSEVIER

Sensors and Actuators A 97–98 (2002) 253–263

SENSORS AND ACTUATORS A PHYSICAL

www.elsevier.com/locate/sna

A robust flow sensor for high pressure automotive applications

U. Schmid*

Department SC/IRT/LG-MX, EADS Deutschland GmbH, 81663 Munich, Germany

Received 12 June 2001; received in revised form 23 November 2001; accepted 28 November 2001

Abstract

In this paper, a micromachined mass flow sensor mounted on a high pressure stable substrate is presented to measure on board the different injection quantities needed in modern direct injection (DI) systems for optimum performance of the engine. To detect the injection end/begin as well as the injection rate as precisely and fast as possible, the sensor is completely integrated into the nozzle body close to the injection holes for the first time. The thermal measurement principle is chosen, as gasoline and diesel fuel quantities can be detected and therefore, the use of this present flow sensor is not restricted to one of these different types of combustion engines. The fabrication process of the molybdenum (Mo) thin film sensors on an LTC (low temperature co-fired) ceramic chip is described. Additionally, FEM simulations concerning the velocity profile in the injection nozzle are performed and the electrical heating power of the hot film anemometer at different overheat ratios is analytically calculated. Finally, the injection rate measurements up to 60 MPa (600 bar) with the nozzle-integrated thin film sensor are presented and their additional information compared to signals gained from an injection amount indicator (EMI), which is part of the high-pressure hydraulic test bench, are discussed.

Keywords: Injection system; Mass flow sensor; Micromachined; High pressure; LTC-ceramics; On-board diagnosis

1. Introduction

In the last years, increasing sales quantities for gasoline as well as diesel passenger cars, which are equipped with a direct injection (DI) system, have been reported [1,2]. This is mainly due to both a permanently increasing fuel price and a growing awareness of the public for environmental problems [3]. Consequently, fuel economy has become a major selling point for car buyers desiring simultaneously a reduced CO_2 emission and a higher output power in the new developed automobiles. But, under all these different DI systems, which are developed to series by the leading car manufacturers, the common rail (CR) injection concept has gained much attention because it offers a fuel injection pressure ranging nowadays for diesel engines up to 1350 bar (135 MPa) being almost independent of load condition, number of revolutions of the camshaft or the geometry of the cam [4]. Therefore, pilot and post injections consisting only of very small fuel quantities, but strongly needed for an optimum performance of the engine, can be realized, especially when a high dynamic piezo-electric driven actuator instead of a magnetic valve is used [5]. To take advantage of the significant potential on the area of injection technology for a further development of the engine, an on-board mass flow sensor is recommended enabling a closed-loop control of the injection rate. This could allow to inject in a reproducible and controlled way even very small fuel quantities. Therefore, a micromachined hot film anemometer placed on a pressure stable ceramic substrate is integrated in the nozzle body close to the injection holes for the first time. This present paper mainly focuses on FEM (finite element method) simulations performed with the software tool Flotran/ANSYS 5.5 on the velocity field in the nozzle. Therefore, analytical calculations allow to estimate the maximum electrical heating power P of the micromachined flow sensor during operation at a possible fuel injection pressure of 135 MPa for diesel engines. Finally, first injection rate measurements at different drive pulses up to 60 MPa, performed with the nozzle integrated flow sensor, are compared to waveforms, gained from an injection amount indicator (EMI), which is part of a high-pressure hydraulic test bench and yields a completely different measurement technique of the injection rate.

2. Fabrication process of the micromachined hot film anemometer

The thermo-resistive measurement principle has been realized using an electrically heated thin film sensor. This type of flow sensor can be fabricated in a batch process and

* Tel.: +49-89-607-20657; fax: +49-89-607-24001.
E-mail address: ulrich.schmid@eads.net (U. Schmid).

0924-4247/02/$ – see front matter
PII: S0924-4247(01)00869-X

requires no moving parts as the micro turbine sensor (MTS) [6]. Therefore, it is very well suited for the application in gasoline as well as diesel engines. Especially for the present application, the hot film anemometer has to be placed on a pressure stable substrate, which is electrically isolating and, with regard to a latter mass production, as cheap as possible. An LTC (low temperature co-fired) ceramics is used, because the fabrication process of the latter allows in addition the integration of electrical feedthroughs with a low resistivity (see Fig. 1). The sintered thick film paste exhibits ohmic behavior and adds in the present design a negligible parasitic resistance of about 100 mΩ to the sensor resistance of about 115 Ω at room temperature. In Fig. 2, a schematic overview of the fundamental technology steps necessary to realize a multilayer glass–ceramic substrate is given, whereas a more detailed description of the latter can be found in [7]. The original soft state of the foil (''green tape''), basically a ceramic powder held together in sheet form by a temporary organic binder, is first pre-baked at about 120 °C to effuse part of the latter. Next, the tape is cut into size and additionally, orientation marks are created for aligning the subsequent process steps to each other. Vias holes are mechanically punched or via lasers drilled into each layer and filled with a conductive metal paste by screen printing technique. A possible printing of conductors is also performed by standard thick film screen printing on each foil, whereas the pastes are specially designed to have almost the same shrinkage of about 12% as the tape. The lamination process comprises a sophisticated pressure as well as heat treatment to the assembly to prepare the different layers for the sintering process in an air furnace. Co-firing is performed between peak temperatures of about 850 °C, preceding a complete organic burnout between 200 and 500 °C, respectively. At least, all electrical components are electrically tested by a 100% final inspection. To simplify the handling of the sample, the ceramic plate with final dimensions of 58 mm × 58 mm is cut into nine pieces, having up to 16 chips, as schematically shown in Fig. 3a. Before the 110 nm thick molybdenum (Mo) thin film is e-beam evaporated on the glass–ceramic substrate, the surface roughness is reduced by mechanical polishing with three different emulsions, having different grain sizes of 3 and 1 μm, respectively, from about ±850 μm (±22%) by more than one order of magnitude to about ±70 nm (±27%). This represents the lowest values achieved in this work on LTCC glass–ceramic tapes, as they are composite materials of about 50% ceramic filler (mostly Al_2O_3) and 50% glass, respectively [8]. As Al_2O_3 particles are uncontrolled and detached during the different polishing procedures, the surface roughness is inhomogeneous over the surface, verified with SEM (scanning electron microscope) pictures (see Fig. 3b), but acceptable for our application. It should be noted that due to different shrinkage coefficients of the green foil and the conductive thick film paste, bumps with a height of about 3.5 μm occur above the electrical feedthroughs after the co-firing process, as shown in Figs. 3b and 4a, respectively. After the complete polishing procedure, however, a trough with rounded edges was measured at this location, as the feedthroughs are polished faster than the surrounding LTC-ceramics (see Fig. 4b). Next, the resulting sensor structures are protected by a 6 μm thick photo resist (AZ4562) for the wet-etching process in aqua regia at room temperature. Finally, the sensor chips are cut out of the glass–ceramic plate with the desired dimensions by an in-house available ultrasonic milling process

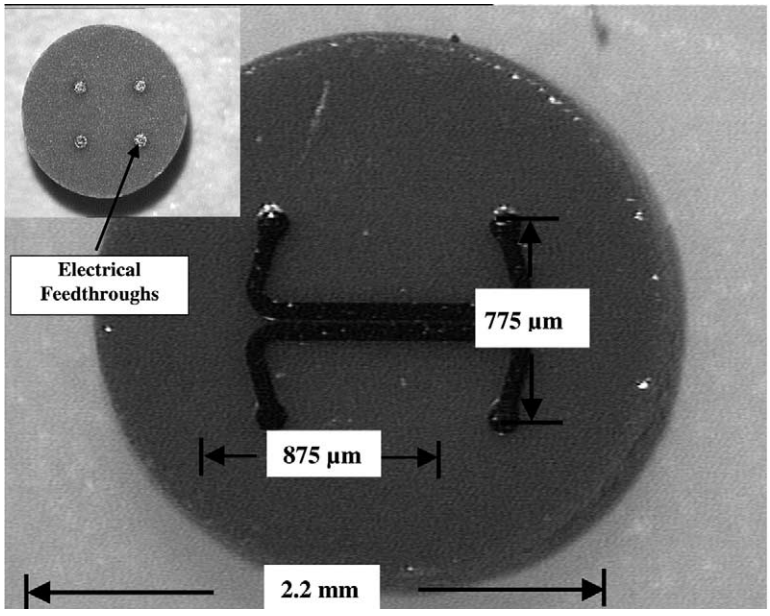

Fig. 1. Top view of two thin film sensors (width $w = 100$ μm, length $L_s = 1.4$ mm), separated by a 10 μm gap. The small picture shows the backside of the ceramic chip (2.2 mm in diameter) with the four integrated electrical feedthroughs contacting the two sensors on the front side.

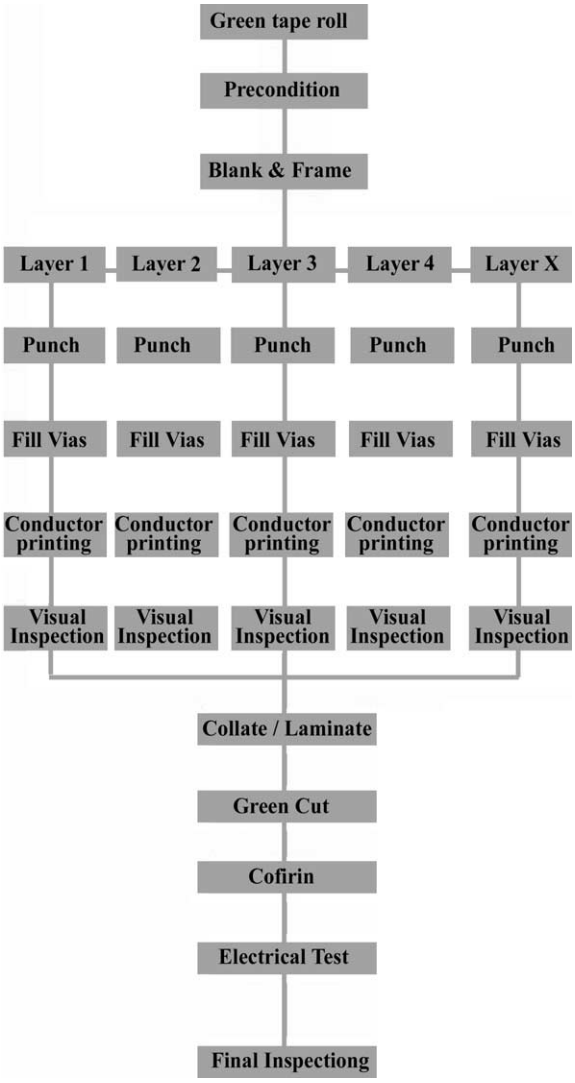

Fig. 2. Schematic flow chart, yielding the most important technology steps to fabricate an LTC (low temperature Co fired) ceramics.

operating at 20 kHz. For a detailed overview, the whole fabrication process is summarized in a schematic flow chart in Fig. 3b.

3. FEM simulations and analytical calculations

In this section, the electrical heating power P of the thin film anemometer is estimated by an analytical model describing a flat plate exposed to turbulent flow. Therefore, in a first step, finite element method (FEM) calculations, employing the software tool Flotran/ANSYS 5.5, are performed and the velocity field close to the nozzle body at a maximum rail pressure of 135 MPa for diesel injection systems is calculated. Thus, the heat transfer coefficient h, which determines the energy loss into the moving fluid, can be analytically deduced. Fig. 5 shows a schematic picture of the geometry used for the present FEM simulations. To save computation time, 2D simulations, using the standard element type Fluid141, have been done. A constant pressure of 135 MPa is applied over the whole cross-section of the gap between the nozzle body and the needle representing the high-pressure side of the injection system. At the injection hole, a pressure of 6 MPa arising from the combustion process is assumed. Only these two boundary conditions at the inlet and the outlet respectively are needed if incompressible flow is studied as in the present case. As high fuel velocities in the nozzle and hence high Reynolds numbers are expected, the standard k–ε model is used to assume the turbulence energy as well as the turbulent dissipation which are not experimentally known. The nozzle body and the needle are regarded as fixed in these steady state considerations and modeled by the boundary condition $v_x = v_y = 0$. Additionally, the model is made large enough to place the sensor sufficiently far away from the inlet to exclude any influences arising from a non-developed velocity profile. Fig. 5 also yields the loss of pressure across the considered inner geometry of the nozzle, where a region with negative pressure occurs at the sharp edge where the injection hole starts. This is due to the limited physical model implemented in Flotran/ANSYS 5.5 regarding a possible changing state of aggregation of the fluid. But, this location with a negative pressure indicates a sever cavitation problem due to a strong change of flow direction. To demonstrate that all these simplifications and assumptions still lead to useful results, the FEM calculations are compared to experimental data on measured injection velocities carried out with a Bosch-type rate of injection flow bench at 120 MPa [9]. A rough estimation yields the injection velocity of the fuel $v_{135\,\mathrm{MPa}}$ at 135 MPa from $v_{120\,\mathrm{MPa}} \approx 450\ \mathrm{m\,s^{-1}}$ according to [10]:

$$v_{p_2} = \sqrt{\frac{p_2}{p_1}} v_{p_1} \quad \text{with} \ \ \rho_1 = \rho_2 \tag{1a}$$

$$\Rightarrow v_{135\,\mathrm{MPa}} = \sqrt{\frac{135\,\mathrm{MPa}}{120\,\mathrm{MPa}}} v_{120\,\mathrm{MPa}} \approx 480\,\mathrm{m\,s^{-1}} \tag{1b}$$

where ρ_1 and ρ_2 denote the densities of the fluid at pressures p_1 and p_2, respectively. The fuel velocities calculated with the FEM software tool yield a maximum value of about $390\ \mathrm{m\,s^{-1}}$ at the injection hole, as shown in Fig. 6. Differences of the measured and via FEM calculated results may arise from the assumptions made in both cases as well as different material parameters used for the fuel, slightly different geometries and boundary conditions. Despite our simple model, however, this deviation of less than 23% supports the assumption that the velocity profile of the fuel at the position of the mass flow sensor is sufficiently well determined. The resulting fuel velocities across the cross-section of the gap between needle and nozzle body are shown in Fig. 7. As expected, the velocity profile is almost perfectly rectangular with a maximum value of about $118\ \mathrm{m\,s^{-1}}$. For the present measurement principle, however, the fuel velocities close to the nozzle body mainly influence

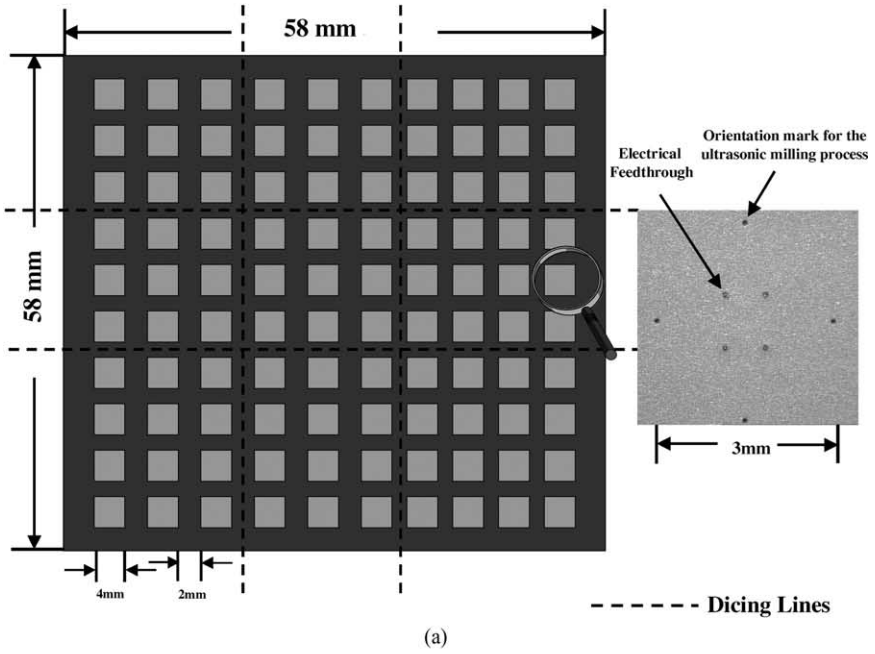

(a)

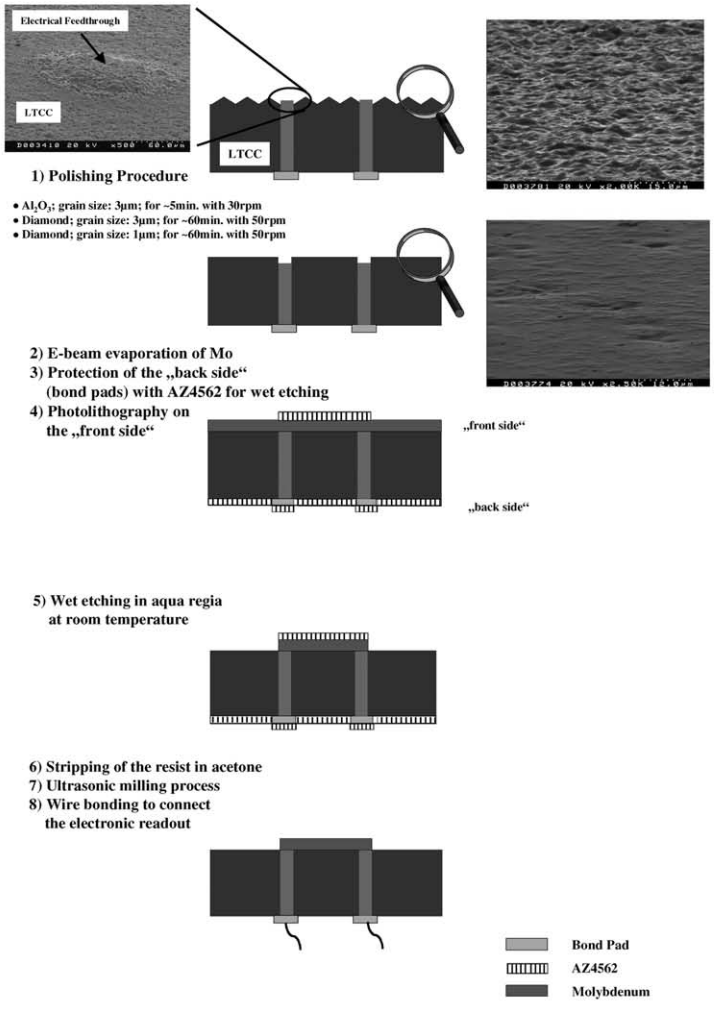

(b)

Fig. 3. (a) Schematic top view on the present design of the LTC ceramic plate; (b) schematic flow chart of the fabrication process of the hot film anemometer.

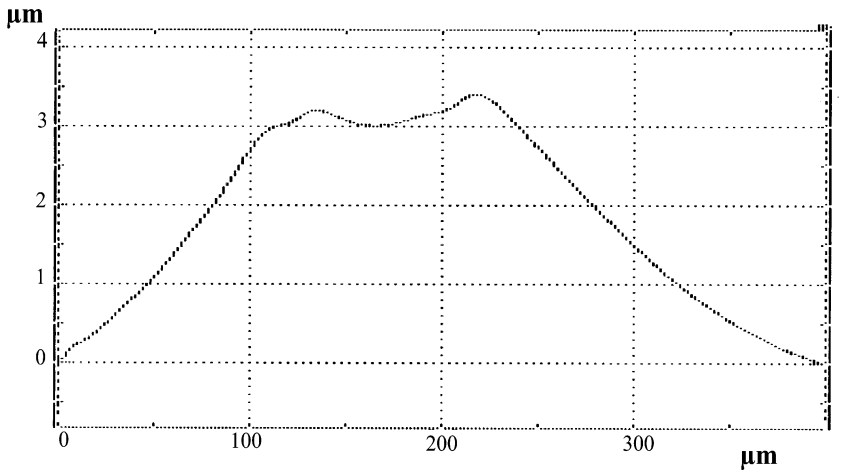

(a)

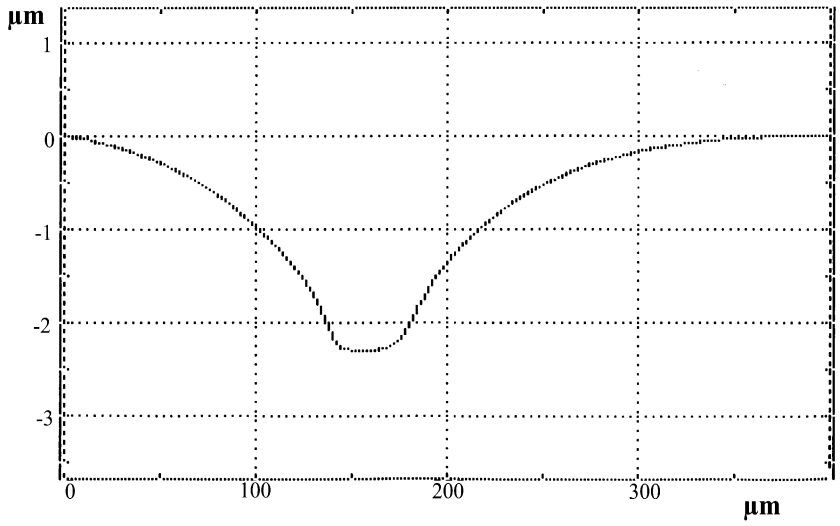

(b)

Fig. 4. (a) Step height measurement done across the unpolished surface of the electrical feedthroughs; (b) step height measurement done across the surface of the electrical feedthroughs after the polishing procedure.

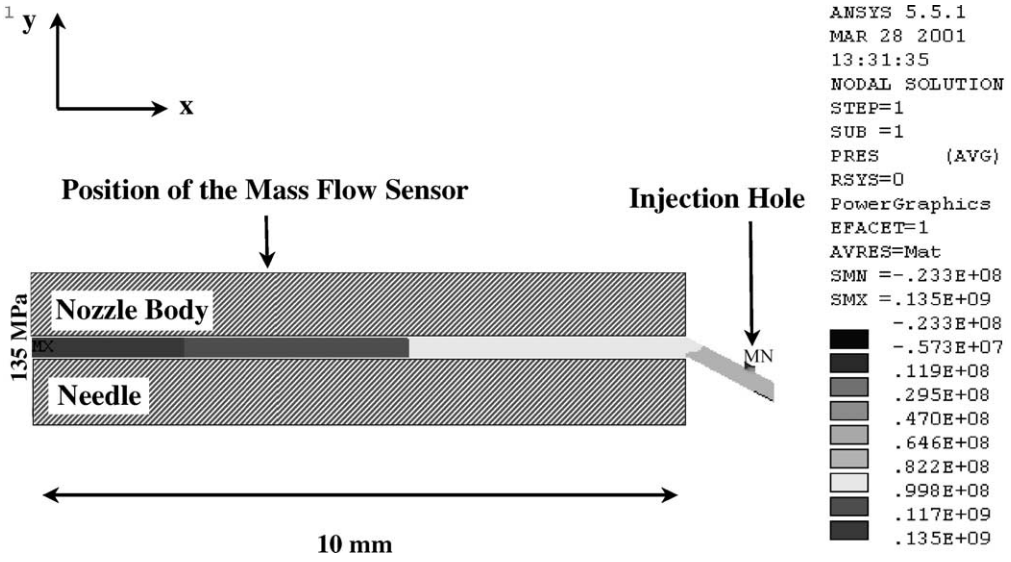

Fig. 5. Calculated loss of pressure across the inner geometry of an injection nozzle. The gap between needle and nozzle wall is 300 µm and the diameter of the injection hole is 150 µm. All material parameters (see the text) for the fluid are assumed to be constant at an ambient temperature of 80 °C.

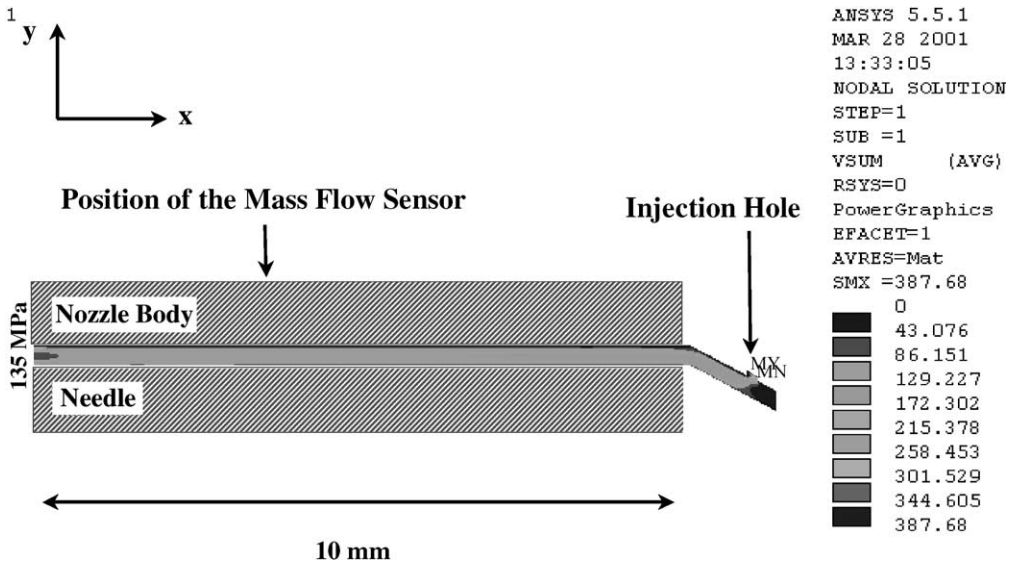

Fig. 6. Absolute value of the calculated velocity profile in the nozzle at an inlet pressure of 135 MPa and an outlet pressure of 6 MPa, respectively. All data are given in SI units.

the heat transfer coefficient h and hence the heat loss to the moving fluid. This detailed investigation requires a fine and mapped meshing close to the wall to get in addition an acceptable convergence of the calculated quantities (e.g. pressure and velocity of the fluid). The velocity in x-direction, according to global Cartesian coordinate in Fig. 5, is additionally shown in the inset of Fig. 7. In distances below 1 μm from the nozzle body fuel velocities of more than $v_{\min,135\,\mathrm{MPa}} = 6\ \mathrm{m\ s^{-1}}$ occur which lead to high sensor signals during operation via an effective and fast cooling of the thin film resistor. The velocity in y-direction close to the nozzle body at the given position of the sensor is more than 300 times smaller than the x-component and hence can be neglected. With the knowledge about the velocity profile at the present sensor position, the electrical heating power P can be estimated assuming for this type of mass flow sensor a flat plate exposed to turbulent flow. In addition to the formula presented for this case in relevant literature [11],

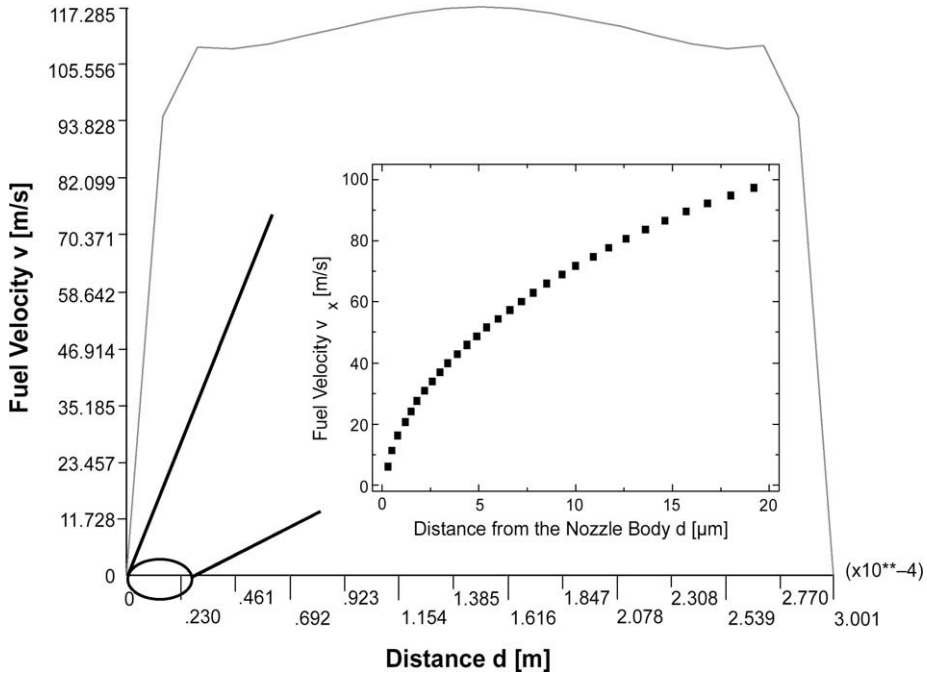

Fig. 7. Absolute value of the calculated velocity profile v across the gap at the marked position of the mass flow sensor (see Fig. 5). A detailed view on the velocity component in x-direction close to the nozzle body and for the present hot film anemometer mainly responsible for the heat transfer to the fluid is depicted in the inset.

the heat loss to the robust LTC-ceramic substrate has to be taken into account. From previous published measurements with an IR imaging system, this part of the total heat flow from the thermal sensor can be determined [12]. Neglecting any radiation and free convection terms to the environment, the following slightly modified equation is gained

$$P = U_s I_s = \left[\frac{\lambda_f}{w} 0.664 \sqrt[3]{\frac{c_f v_f \rho_f}{\lambda_f}} \sqrt{\frac{2 d_{gap}}{v_f}} v (2 d_s L_s + A_s) + \lambda_k \frac{A_s}{d_k} \right] (T_s - T_a) \quad (2)$$

where U_s is the voltage across the thin film sensor, I_s the current through the thin film sensor, ρ_f the fluid density (=848 kg/m^3), v_f the dynamic viscosity (= 5.3×10^{-6} m^2 s^{-1}), λ_f the heat conductivity of the fluid (=0.11 W m^{-1} K^{-1}), c_f the specific heat capacity of the fluid (=2300 J kg^{-1} K^{-1}), d_s the thickness of the thin film (=100 nm), L_s the length of the thin film sensor (=1.4 mm), w the width of the thin film sensor (=100 μm), A_s the area of the thin film sensor ($=L_s w$), T_a the ambient fluid temperature, T_s the temperature of the thin film sensor, λ_k the heat conductivity of the LTC-ceramics (=3 W m^{-1} K^{-1}), d_k the characteristic penetration depth of the static temperature field into the LTC-ceramics (=130 μm) [12].

It should be noted that the fluid density and the dynamic viscosity are considered at an ambient temperature of 80 °C and the values for the sensor design for these calculations are taken from the layout used to fabricate the hot film anemometer presented in Fig. 1. Mainly due to the high velocities and the pressure stable ceramic substrate, the electrical heating power, as shown in Fig. 8, is relatively high compared to thermal mass flow sensors on a membrane structure for gas detection [13]. On the other hand, a sensor temperature below 200 °C is recommended to minimize dirt deposits from the fuel on the hot film anemometer leading to enhanced drifts of sensor constants [14]. Therefore, at $v_{min,135\,MPa} = 6$ m s^{-1} representing the minimum calculated fuel velocity at the nozzle body and at a maximum temperature difference of 120 °C at $T_a = 80$ °C, P of about 1.8 W must be supplied to the thermal mass flow sensor, according to Fig. 8.

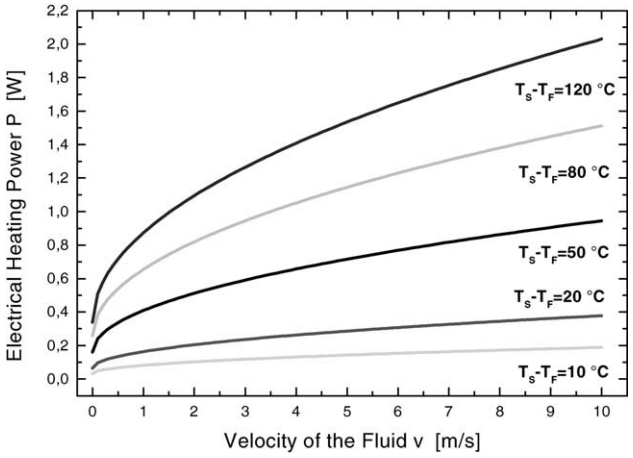

Fig. 8. Electrical heating power P vs. velocity of the fuel v at different sensor temperatures T_s according to Eq. (2). Note that a certain offset occurs at $v = 0$ m s^{-1} due to the heat loss to the LTC-ceramics.

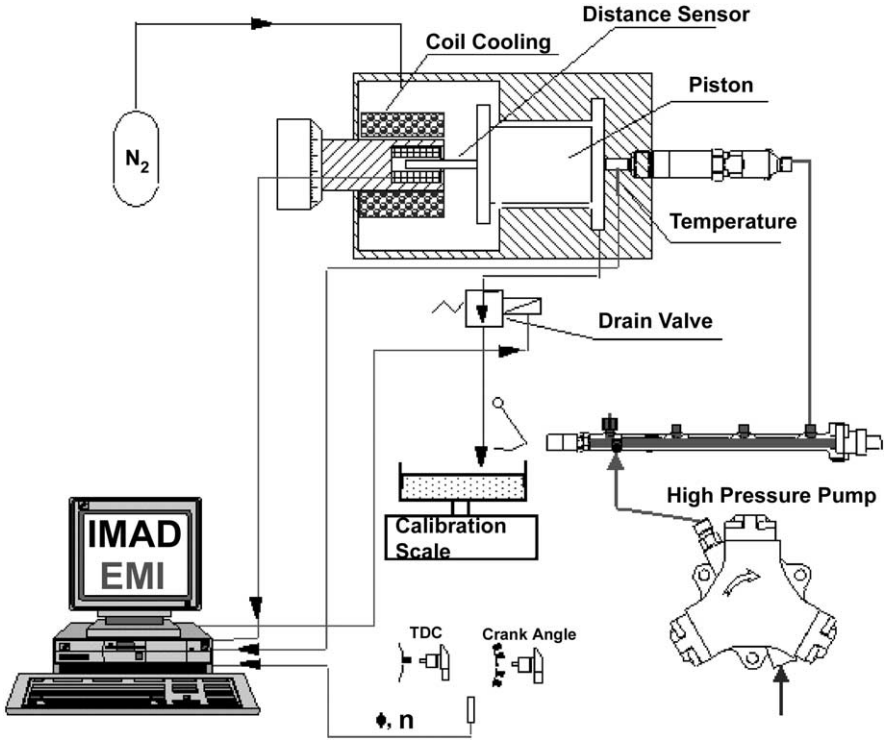

Fig. 9. Schematic overview of the injection test bench.

4. The high pressure hydraulic test bench

For the hydraulic evaluation of injection systems, volume measurements have to be performed at an injection test bench. Therefore, a complete injection system is setup with all motor boundary conditions. The test bench can be subdivided into the following main components:

- injection system;
- electric motor (propulsion of the high-pressure pump);
- sensors for number of revolutions, rail pressure, needle stroke and temperature;
- control unit for the injection system;
- test bench control system;
- injection amount indicator (EMI);
- measurement data recording (IMAD).

The main component of the injecting test bench is the injection amount indicator (EMI). With the latter, it is possible to measure the quantity brought in per injection temporally dissolved. By differentiating the measured signal the injecting rate is gained. The measurement data recording (IMAD) controls the test bench and is connected by an interface with the control unit of the injection system. Because of the coupling of the test bench with the injection system, it is possible to perform injection quantity measurements with

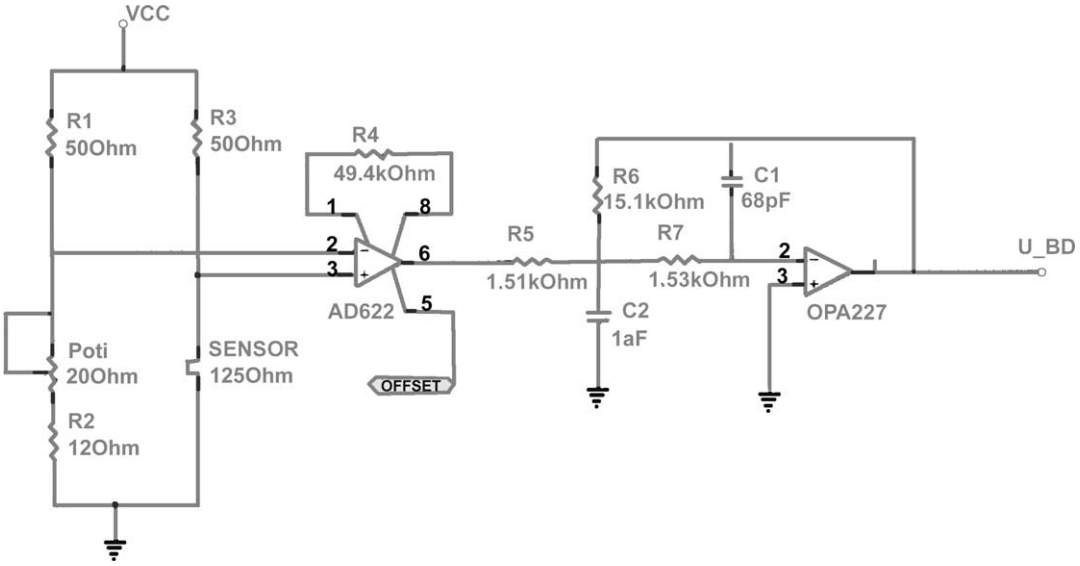

Fig. 10. Circuit diagram showing the mass flow sensor in the Wheatstone bridge and the subsequent electronic readout. V_{cc} is 5 V and the voltage drop across the sensor is measured to be 3.5 V at the operating point.

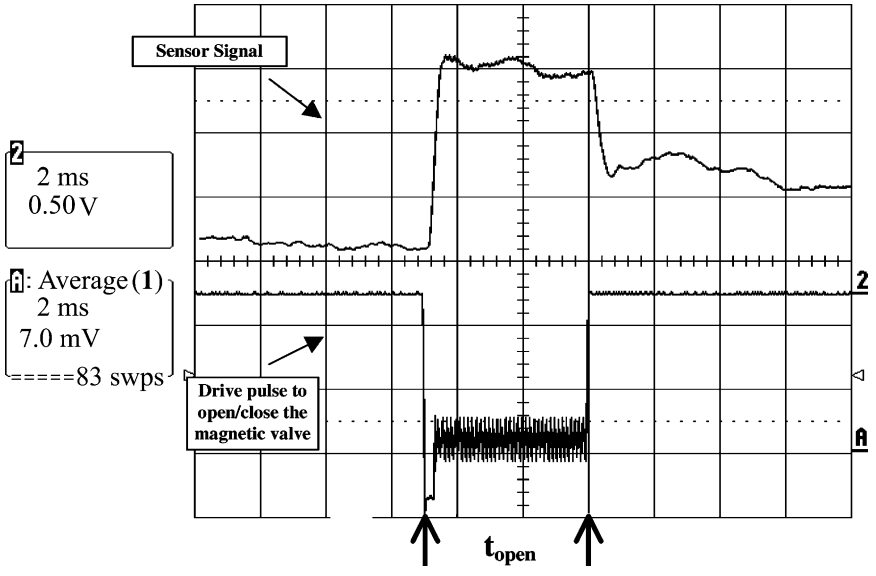

Fig. 11. Amplified (gain $G = 2$) and filtered sensor signal at $t_{open} = 5$ ms with an amplitude of about 19 mV at 20 MPa.

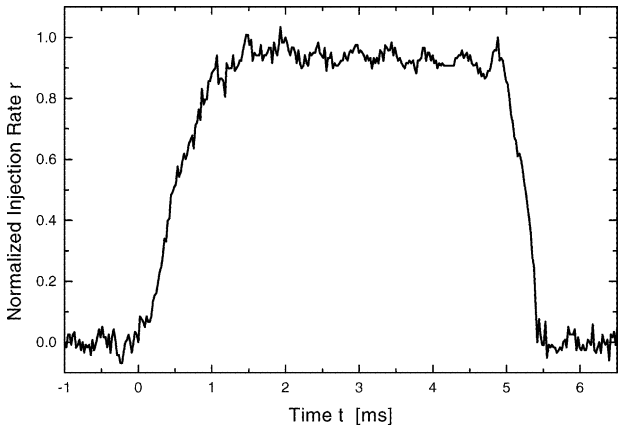

Fig. 12. Normalized injection rate r vs. time t at a drive pulse of $t_{open} = 5$ ms at 20 MPa, determined with the injection amount indicator (EMI/IMAD).

characteristic maps. An overview of the injection test bench is shown in Fig. 9. The fuel quantity, coming out of the nozzle at each stroke, is determined inductively by a moving piston in a water cooled coil. As the displacement of the piston is proportional to fuel quantity, a subsequent differentiation yields the injection rate r. On the rear side of the piston a nitrogen pad exists to simulate the compression pressure arising in the engine. After each injection, the measuring chamber is emptied using a drain valve.

5. Injection rate measurements and hydraulic simulations of the injection rate up to 60 MPa

In this section, the first injection rate measurements at rail pressures up to 60 MPa at different drive pulses, carried out with the design of the mass flow sensor, presented in Section 2, and performed at the high pressure test bench, are presented. In a further step, these injection rate measurements are compared to the data, gained from the EMI/IMAD system (see Section 4). The signals of the micromachined sensors are read out by a Wheatstone bridge followed by an amplification and filtering unit, whereas the latter is designed to have its corner frequency (−3 dB) at about 100 kHz. This effectively reduces in the electronic readout the electronic noise arising mainly from the high-pressure pump unit, but has negligible influence on the sensor signals below 1 kHz. A schematic circuit diagram is shown in Fig. 10. Fig. 11 shows at a rail pressure of 20 MPa the drive pulse to open the magnetic valve as well as the resulting change resistance of the micromachined hot film sensor, represented by the diagonal bridge voltage due to the fuel mass flow. Pressure waves occurring during and after the injection pulse are clearly measurable and arise from the fast acceleration and deceleration at the injection begin and end, respectively. In Fig. 12, the corresponding waveform of the EMI/IMAD system at a rail pressure of 20 MPa and a drive pulse of 5 ms is shown. Especially these information about the flow condition, concerning the time after the nozzle is closed by the needle, are experimentally gained with such a nozzle-integrated flow sensor, as the EMI/IMAD system provides only a signal of the injection rate, when a net mass flow exists out of the nozzle. The high frequency oscillations in Fig. 12, however, result mainly from a non-optimized damping of the moving piston in the coil and are superimposed to the pressure waves, affecting the injection rate [15]. The rise time t_{rise} defined as the time period until the curves of all three different techniques to determine the injection rate have reached 90% of their full output swing, is for the mass flow sensor about 0.6 ms (see Fig. 11) and about

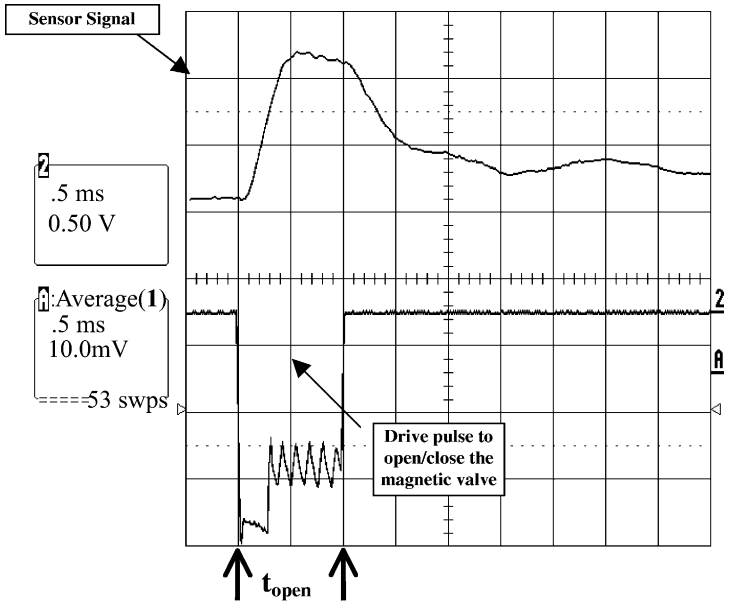

Fig. 13. Amplified (gain $G = 2$) and filtered sensor signal at $t_{open} = 1$ ms with an amplitude of about 24 mV at 60 MPa.

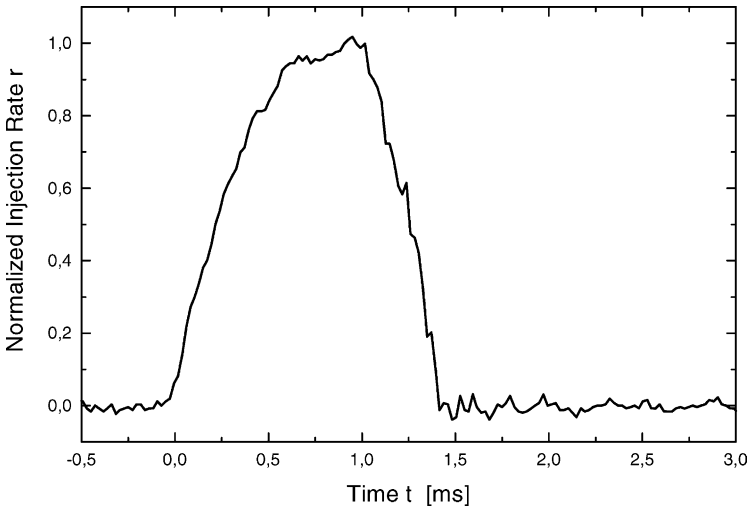

Fig. 14. Normalized injection rate r vs. time t at a drive pulse of $t_{open} = 1$ ms at a rail pressure of 60 MPa, determined with the injection amount indicator (EMI/IMAD).

1.1 ms for the EMI signal (see Fig. 12) at 20 MPa, respectively. But, regarding the measurement technique of the latter, where the displacement of a piston in a coil is read out inductively, a higher rise time is expected than for the robust hot film anemometer due to the integration of the latter directly into the injection nozzle. The low t_{rise}, associated with the mass flow sensor, shows its high sensitivity to the accelerated fuel column due to its small mass and enables with an equivalent fall characteristic at the closing of the valve a fast and precise detection of the injection begin and end, respectively. Additional to the wavy characteristics, the signal height of the micromachined mass flow sensor is slightly decreasing during injection, which is in this graph equivalent with a subsequent heating of the thin film resistor (see Fig. 11). This is due to the thermal time constant τ of the underlying LTC-ceramic substrate being in the 3–4 ms range [16] and which heats during operation the presently cooler sensor. This phenomenon is of course also observed, when the fuel injection pressure is increased to 60 MPa and simultaneously the drive pulse is decreased to 1 ms, as shown in Fig. 13. Again, a decreasing height of the sensor signal is measured during injection and pressure waves in the nozzle prevent after the closing procedure the Wheatstone bridge signal to reach the working point not before a time span of about 20 ms. The rise time t_{rise} is measured at a rail pressure of 60 MPa to about 0.4 ms by the micromachined flow sensor (see Fig. 13) and to about 0.6 ms by the EMI/IMAD system (see Fig. 14). The shorter values for t_{rise} compared to a fuel pressure of 20 MPa are due to a faster lift of the needle by higher hydraulic forces and also an enhanced heat transfer from the hot film anemometer into the fluid by higher fuel velocities. The electrical heating power $P = 100$ mW corresponds for this present sensor design to a thin film temperature of about 70 °C at a closed-loop controlled fluid temperature of 40 °C. For the first tests, a low heating power was chosen to prevent the thin film resistor from an early failure. According to [17], the change in sensor resistance ΔR_s can be calculated via the amplitude of the diagonal bridge voltage. As material parameters of thin films strongly differ from those measured at large, crystalline samples (bulk) [18], the temperature coefficient of resistance of 100 nm thick molybdenum thin films between room temperature and 200 °C on the glass–ceramic substrate are determined to $\alpha_{473} = 9.3 \times 10^{-4}\ K^{-1}$ [12]. Finally, the change in sensor temperature ΔT_s during operation can be calculated to about 10 K at 200 bar ($t_{open} = 5$ ms) and about 13 K at 600 bar ($t_{open} = 1$ ms), respectively. Note, that the increased signal height at 60 MPa, compared to a rail pressure of 20 MPa, is due to a higher convective heat transfer into the fluid and hence, to higher decrease in sensor temperature.

6. Conclusion

In this work, a description of the fabrication process of a thermal mass flow sensor, designed to operate under high-pressure environmental conditions, is presented. FEM simulations are performed with the software tool Flotran/ANSYS 5.5 to calculate the velocity profile in the injection nozzle at a fuel pressure of 135 MPa. Comparing these results of the fuel velocities at the injection holes to those, which are measured at the tip of the nozzle with a Bosch-type rate of injection flow bench, a quite good correspondence is gained despite the simplifying assumptions in the FEM simulations regarding the pressure-dependency of the density and the viscosity of the fuel. Assuming, that the velocity profile at the position of the hot film anemometer is also correctly determined with the FEM simulations, the electrical heating power during operation can be analytically calculated. The latter is for a maximum overheat ratio ($T_s/T_a < 2.5$) in oil atmosphere at an ambient temperature of $T_a = 80$ °C well

below 2 W for the discussed sensor design ($A_s = 1.4 \times 10^{-7}$ m^2), which is feasible on board of an automobile. Injection rate measurements at 20 and 60 MPa at different drive pulses of 5 and 1 ms, respectively are presented and discussed. A comparison of these measurements to those, performed with an amount injection indicator (EMI) demonstrates the high performance of the hot film anemometer during operation. Outstanding advantages of the nozzle integrated thin film sensor are its fast response to any changes of the fuel mass flow in the nozzle compared to the mechanical setup of the EMI/IMAD system and the possibility, to gain experimentally information about the flow condition in the nozzle even after the end of the injection pulse, when no net mass flow exists out of the injection holes. This demonstrates for the first time, that it is technologically feasible to integrate micromachined flow sensors directly into the body of a common rail injection nozzle, to close loop control in a further step the injection quantity. Future work has mainly to focus on a proper passivation layer to minimize dirt deposit from the fuel on the surface of the thermal sensor as well as lifetime test in diesel/gasoline atmosphere. These first results, however, demonstrate the excellent performance of this measurement technique for high-pressure automotive applications and it is believed, that such robust sensors will substantially contribute in the future to a further optimization of the combustion process.

Acknowledgements

The author wishes to thank Dr. G. Renner (Department EP/MDH at the DaimlerChrysler AG), Mr. Poschner (FT1/MP at the DaimlerChrysler AG) and Dr. M. Eickhoff (Technical University of Munich) for valuable discussions and their support.

References

[1] K. Egger, D. Schöppe, Diesel common rail II—Injection technology for the challenges of the future, in: Proceedings of the Wiener Motoren Symposium, Vol. 19, 1998, pp. 290–306.
[2] D. Geurts, B. Schreurs, M. Peters, A cost effective concept for meeting EURO IV with traditional port fuel injection systems, in: Proceedings of the IMechE Seminar on the EUROP IV Challenge—Future Technologies and Systems, London, December 1997, pp. 3–4.
[3] H. Eichlseder, E. Baumann, P. Müller, S. Rubbert, Gasoline direct injection—a promising engine concept for future demands, in: Proceedings of the SAE World Congress, Detroit, 2000, No. 2000-01-0248.
[4] K.H. Hoffmann, K. Hummel, T. Maderstein, A. Peters, Das common-rail einspritzsystem—ein neues kapitel der dieseleinspritztechnik, MTZ 58 (1997) 572–582.
[5] J. Willand, J. Haag, G. Renner, U. Engel, K.H. Hoffmann, The piezo-actuator as future control device for HSDI-common-rail-systems, in: Proceedings of the Wiener Motoren Symposium, Vol. 19, 1998, pp. 237–349.
[6] T. Iwasaki, H. Maehara, O. Berberig, K. Nottmayer, T. Kobayashi, Study of a sensor for fuel injection quantity, 1997, SAE Paper No. 970533.
[7] http://www.national.com/appinfo/ltcc.
[8] R. Gongora-Rubio, P. Espinoza-Vallejos, L. Sola-Laguna, J.J. Santiago-Aviles, Overview of low temperature co-fired ceramics-tape technology for meso-system technology (MsST), Sens. Actuat. A 89 (2002) 222–241.
[9] P.J. Tennison, T.L. Georjon, P.V. Farrell, R.D. Reitz, An experimental and numerical study of sprays from a common rail injection system for use in an HSDI diesel engine, 1998, SAE Paper No. 980810.
[10] H. Kuchling, Taschenbuch der Physik, Fachbuchverlag Leipzig, 1986, ISBN 3-343-00759-5.
[11] Berechnungsblätter Für den Wärmeübergang, Vol. 7, Auflage, VDI Wärmeatlas, 1994, ISBN 3-18-401361-8.
[12] U. Schmid, G. Krötz, H. Öing, G. Renner, D. Schmitt-Landsiedel, A flow sensor for harsh environmental automotive applications, in: Proceedings of the 10th International Conference on Sensor 2001, Vol. 1, Nuremberg, May 2001, pp. 25–30.
[13] T. Neda, K. Nakamura, T. Takumi, A polysilicon flow sensor for gas flowmeters, in: Proceedings of the Eighth International Conference On Solid State Sensors and Actuators (Transducers'95), 1995, pp. 548–551.
[14] H. Eckelmann, Hot wire and hot film measurements in oil, DISA Info. 13 (1972) 16–22.
[15] Poschner, Private Communication (FT1/MP), DaimlerChrysler AG.
[16] U. Schmid, G. Krötz, R. Hoffmann, D. Schmitt-Landsiedel, A thermal flow sensor for common rail injection systems, in: Proceedings of the 11th International Conference On Solid State Sensors and Actuators (Transducers'01), 2001, pp. 1452–1455.
[17] P. Freymuth, Frequency response and electronic testing for constant-temperature hot-wire anemometers, J. Phys. E. Sci. Instr. 10 (1977) 705–710.
[18] T.J. Coutts, Electrical Conduction in Thin Metal Films, Elsevier, Amsterdam.

Biography

U. Schmid was born in Munich, Germany, in 1972. He started studies in physics and mathematics at the University of Kassel in 1992. In 1995, he spent 6 months at the Transport Group in the Physics Department, University of Nottingham, UK, to gain experience in wide bandgap semiconductor physics. He performed his diploma work at the research laboratories of the Daimler-Benz AG (now DaimlerChrysler AG) on the electrical characterization of silicon carbide junction field effect transistors at high temperatures. During this time, he also investigated metal-oxide-semiconductor (MOSiC) structures such as gate controlled diodes, MOSFETs, and integrated circuits for harsh environment applications. He finished his studies with the "Vordiplom" in mathematics and the "Diplom" in physics in 1998 at the University of Frankfurt, Germany. Since 1999, he is pursuing the Ph.D. degree at the DaimlerChrysler AG (now EADS Deutschland GmbH), Munich, on mass flow sensors for high pressure automotive applications.